applied sciences

MDPI

Review

Recognition of Driving Behavior in Electric Vehicle's Li-Ion Battery Aging

Ka Seng Chou [1,2,*], Kei Long Wong [1], Davide Aguiari [2,3], Rita Tse [1], Su-Kit Tang [1] and Giovanni Pau [2,3,4]

[1] Faculty of Applied Sciences, Macao Polytechnic University, Macao SAR 999078, China; keilong.wong@mpu.edu.mo (K.L.W.); ritatse@mpu.edu.mo (R.T.); sktang@mpu.edu.mo (S.-K.T.)
[2] Department of Computer Science and Engineering, University of Bologna, 40126 Bologna, Italy; davide.aguiari2@unibo.it (D.A.); giovanni.pau@unibo.it (G.P.)
[3] Autonomous Robotics Research Center, Technology Innovation Institute (TII), Abu Dhabi P.O. Box 9639, United Arab Emirates
[4] Samueli Computer Science Department, University of California, Los Angeles, CA 90095, USA
* Correspondence: kaseng.chou@mpu.edu.mo

Abstract: In the foreseeable future, electric vehicles (EVs) will play a key role in the decarbonization of transport systems. Replacing vehicles powered by internal combustion engines (ICEs) with electric ones reduces the amount of carbon dioxide (CO_2) being released into the atmosphere on a daily basis. The Achilles heel of electrical transportation lies in the car battery management system (BMS) that brings challenges to lithium-ion (Li-ion) battery optimization in finding the trade-off between driving and battery health in both the long- and short-term use. In order to optimize the state-of-health (SOH) of the EV battery, this study focuses on a review of the common Li-ion battery aging process and behavior detection methods. To implement the driving behavior approaches, a study of the public dataset produced by real-world EVs is also provided. This research clarifies the specific battery aging process and factors brought on by EVs. According to the battery aging factors, the unclear meaning of driving behavior is also clarified in an understandable manner. This work concludes by highlighting some challenges to be researched in the future to encourage the industry in this area.

Keywords: lithium-ion battery; battery aging; driving behavior; electric vehicle; machine learning; OBDII; NMC battery

check for updates

Citation: Chou, K.S.; Wong, K.L.; Aguiari, D.; Tse, R.; Tang, S.-K.; Pau, G. Recognition of Driving Behavior in Electric Vehicle's Li-Ion Battery Aging. *Appl. Sci.* **2023**, *13*, 5608. https://doi.org/10.3390/app13095608

Academic Editor(s): Gaind P. Pandey and Jianqiang Kang

Received: 3 April 2023
Revised: 24 April 2023
Accepted: 27 April 2023
Published: 1 May 2023

Copyright: © 2023 by the authors. Licensee MDPI, Basel, Switzerland. This article is an open access article distributed under the terms and conditions of the Creative Commons Attribution (CC BY) license (https://creativecommons.org/licenses/by/4.0/).

1. Introduction

The use of battery electric vehicles (BEVs) will be essential to the decarbonization of transportation networks in the near future. The quantity of CO_2 emitted into the environment each day can be decreased by switching from ICE-powered automobiles to electric ones. However, environmental pressure appears on the heavily polluted manufacturing and recycling processes of the batteries, which generate more than 150 kg hazardous waste per 1 gigawatt-hour [1]. To reduce the contaminants without inventing manufacturing processes and materials, maintaining the battery in optimal operations can best extend the battery life. However, analyzing the optimal operation windows for the battery in a BEV is challenging. It involves identifying driving behaviors and mapping them to intricate battery aging parameters, including current profile, depth of discharge (DOD), state-of-charge (SOC), and temperature [2].

Recognizing driving behavior is also essential for the BMS to predict the SOH appropriately. The SOC and SOH are currently measured by the BMS using data-driven, model-based (e.g., equivalent circuit, electrochemical, mathematical), and a mixture of both methods [3–5]. In the data-driven approach, BMS can best cooperate with the driving behavior to mitigate battery degradation and optimize the battery life. Furthermore, unhealthy driving behavior can be realized by the driver. When driving operations correlate

to the speed of degradation, the way that people drive in BEVs can be altered in a way that can prolong the battery life.

Compared to ICE vehicles, the BEV industry has yet to reach its full potential for discovering explainable driving behavior. Many of the existing driving classifications are at the application level, which emphasizes aggressive driving as a safety risk in the context of public transit [6–8]. The versatility of the collected vehicle data (e.g., controller area network (CAN) bus, image, gyroscope) is prone to indigestion in the mathematical-based traditional models. Multi-dimensional time-series data are challenging to apply to the majority of statistical models, including hidden Markov model (HMM) [9–14], Gaussian mixture model (GMM) [15–19], support vector machine (SVM) [20–27], Naive Bayes (NB) [28–30], fuzzy logic (FL) [31–36], and k-nearest neighbor (KNN) [20,37–40]. The deep learning based models, including convolutional neural network (CNN) [41–48], recurrent neural network (RNN) [49–60], and Fusion models [61–63], showed extremely accurate classification results, but they were rarely connected to the reasons behind the driving behaviors. In addition, the electric power in BEVs can serve the purpose of some essential driving operations (e.g., acceleration and braking). Consequently, the level of explanation for driving behavior can be increased by recognizing the electric power patterns and reverse mapping from electric power to driving operations.

Previous studies have provided a substantial amount of data on the car battery and driving [64]. However, the integrated data for driving and batteries on real BEVs are still extremely limited, because they can only be collected onboard the BEV with data accessing protocol. Meanwhile, SOH analysis requires the fine-time granularity of the acquired data (e.g., 250 ms sample rate). Currently, internet of things (IoT) devices can perform data collection in various situations and on precise time scales [65]. However, many automotive electronic control units (ECUs) can only operate at a lower sample rate due to the heavy load on the automobile's ECU. Even a substantial dataset gathered via the Chinese EV GB/T 32960.3-(accessed on: 20 March 2023) protocol was unable to achieve the fine-time granularity (i.e., 15 s sampling rate).

Therefore, we offer a summary of research on driving behavior based on the Li-ion battery in BEVs. This work is aimed at summarizing the methods for recognizing driving behavior in an explainable manner in addition to the battery degradation process and the BEV-related degradation factors. Finally, the public dataset that is potentially available for such studies was used . The main contributions are given as follows:

- Analysis of the methods for classifying the driving behavior in an explainable form with conventional and deep learning methods;
- Summary of the battery degradation process and factors caused by BEVs and clarification of the ambiguous definitions of current expert driving or labeling data;
- Overview of the fine-time granularity BEVs data that are publicly accessible.

The organization of this paper's structure is as follows: Section 2 describes the laboratory-discovered degradation process for the typical lithium nickel manganese cobalt oxide ($LiNiMnCoO_2$) (NMC) battery used in mainstream BEV application. The causes and warning signs of the BEV's rapid deterioration due to real-world driving are also provided. In order to identify the lifetime driving activities for battery aging correlations, Section 3 investigated the driving behaviors detection techniques of both traditional machine learning and deep learning. The last part includes the paper's findings and future directions.

2. Battery Degradation Mechanism

There are three varieties of EVs available on the market: BEV, hybrid electric vehicle (HEV), and plug-in hybrid electric vehicle (PHEV) [2]. They all have different batteries (i.e., capacity, chemical characteristics, and degradation mechanisms). For BEV, HEV, and PHEV, the capacity is typically 20 to 80 kWh, 1.3 to 1.6 kWh, and 4.5 to 10 kWh, respectively. The electrochemistry of different EVs and the associated battery types also differ. For example, the $Li_4Ti_5O_{12}$ (LTO) anode material in the battery can provide stronger electrolyte stability than graphite, although it has a lower capacity. Despite having a higher energy

density, the $Li[Ni_xMn_yCo_z]O_2$ (NMC) with graphite material in the battery has a limited lifespan [66]. Only the BEV, the most common EV, and the most widely used battery, which uses the NMC material will be the subjects of this study [67].

Han et al. [66] showed the main elements and degradation mechanisms inside the lithium-ion battery (LiB). Generally, anode and cathode material sheets are intercalated by the current collectors (i.e., copper and aluminum) and isolated by a sheet of separator in the middle. Inside the battery shell, the electrolyte is filled to allow the full conduction of the materials. The structure and NMC materials can provide a high energy density, long cycle life, and exceptional thermal stability, but also poor safety [68]. This is because the electrochemical characteristics of these materials are not stable. They will continue to produce chemical reactions, discharging and charging over time, which will affect the life of the battery. Meanwhile, the battery's minuscule internal short circuit and a rapid spike in heat generation at various SOCs hinder efforts to maximize battery utilization [69,70].

All the electrochemical processes that have been identified as contributing to LiB degradation are outlined in Figure 1. Degradation comes in two forms: capacity fading and power fading. Capacity fading would be the SOH, which can be assessed in a variety of ways [71]. Power fading is determined by Ohm's law and the electric power formula $P = UI = U^2/R$. The power decreases as the battery's internal resistance rises. The next subsections will go into further detail on the reactions.

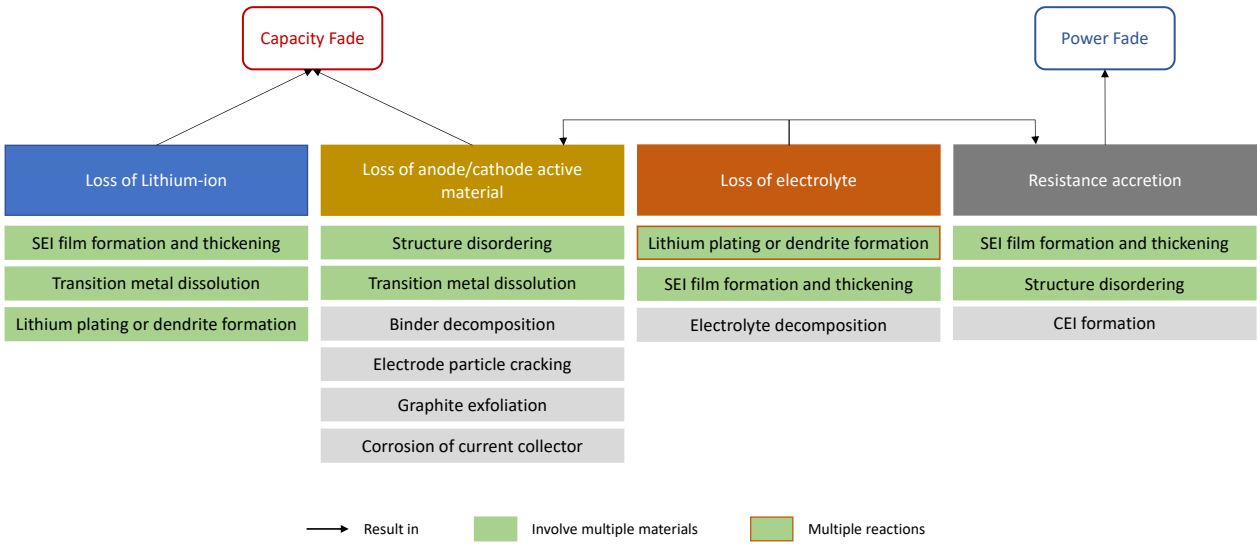

Figure 1. The degradation reactions overview.

Graphite currently makes up the majority of anode active material. The fundamental problem causing the battery's deterioration is the solid electrolyte interphase (SEI) film [72], as illustrated in Table 1. When the LiB is charged for the first time, 5% to 10% of the Li-ions are used up to create a layer between the electrolyte and the graphite that prevents the graphite from coming into touch with the electrolyte and gives the Li-ions a high degree of permeability [73]. This layer is prone to corrosion and will eventually develop fissures. Additionally, cracks appear during charging due to the volume expansion up to 10% of the graphite [74]. According to Guo et al. 2021 [2], the SEI layer cracks would grow larger and faster when the battery was under high DOD and SOC conditions. These fissures will continue to interact with the electrolyte, consuming the Li-ions and generating gas. As a result, the SEI layer's thickness will continue to rise with the capacity loss caused by the reduction of Li-ions.

Table 1. The main degradation mechanisms in anode of the LiB.

Processes	Caused by	Consequence
SEI film [72]	High DOD or high idling SOC	Li-ion consumed and increased thickness, loss capacity directly; easy to corrode and react with electrolyte in the long term;
Dendrites growth [75]	High DOD, SOC, or low temperature	Disorder of the material structure and pieces of the separator, which results in short circuits and thermal runaway
Lithium plating [76]	High SOC or low temperature	Reduction of Li-ion which results in dead lithium and second SEI film irreversibly

The active NMC cathode was first suggested in the 1990s [77]. Currently, many electrochemical processes that contribute to LiB aging have been identified over the decades. The main processes are summarized as following Table 2. Due to the large reduction in Li-ions, cathode–electrolyte interface (CEI) film is one of the processes that contributes most to degradation.

Table 2. The main degradation mechanisms in the cathode of the LiB.

Processes	Caused by	Consequence
Phase transition [78]	High current rate	Irreversible disorder of the cathode structure
Cracking in particles [79]	Long term high voltage or high current	Obstructing Li-ion diffusion, powdering, and collapse of cathode
TMD [80]	High temperature, voltage at high SOC level	Manganese reacts with organic solvents and produces hydrogen fluoride (HF) which will dissolve the transition metals and Li-ions on the surface of the cathode
CEI film [81]	High voltage at high SOC	Li-ions are lost via an interaction with electrolytes that is analogous to the SEI film
Binder decomposition and Collector dissolution [82]	High temperature	An unstable anode structure leads to a loss of electrode contact

The electrolyte maintains the LiB's cycle stability, capacity, and safety between the anode and the cathode [83,84]. Table 3 is a breakdown of the precise electrochemical processes. The mainstream material for BEV is lithium hexafluorophosphate ($LiPF_6$). However, the $LiPF_6$ is unstable and easily breaks down into the lithium fluoride (LiF) and phosphorus pentafluoride (PF_5) depending on the carbonates present (e.g., ethyl methyl carbonate (EMC), dimethyl carbonate (DMC), and diethyl carbonate (DEC)) [85]. Table 3 displays the major electrolyte degradation map. In the presence of high voltage and SOC, the electrolytes dissolve into HF. The CEI film processes can be sped up by the HF since it will corrode the cathode and produce additional ingredients. Certain gases are created when temperatures rise (over 69 °C), which causes electrolyte breakdown [86].

Table 3. The main degradation mechanisms in the electrolyte of the LiB.

Processes	Caused by	Consequence
Electrolyte decomposition [87]	High voltage and SOC	Erode cathode and produce more CEI ingredients
Gas formation [88]	High temperature, voltage, and SOC	An increase of pressure inside the battery by the gas (H_2, CH_4, CO_2, CO) can result in fire and explosion of the battery

Degradation Caused by BEVs

The relationship between the EV and the Li-ion battery's electrochemistry is shown in Figure 2. The EV battery charging process is most closely examined to find any charging parameter flaws. To balance the demands of the consumer with battery optimization, empirical studies are frequently used to design charging techniques. One of the charging methods recognized as the industry standard for the unified charging pole is constant current constant voltage (CC-CV) [2]. Some of the more advanced BMSs also added a delay in charging to regulate the ideal battery pack temperature. Both the voltage and the current are effectively managed. However, the DOD influences the battery cycle, speeding up the battery's aging process.

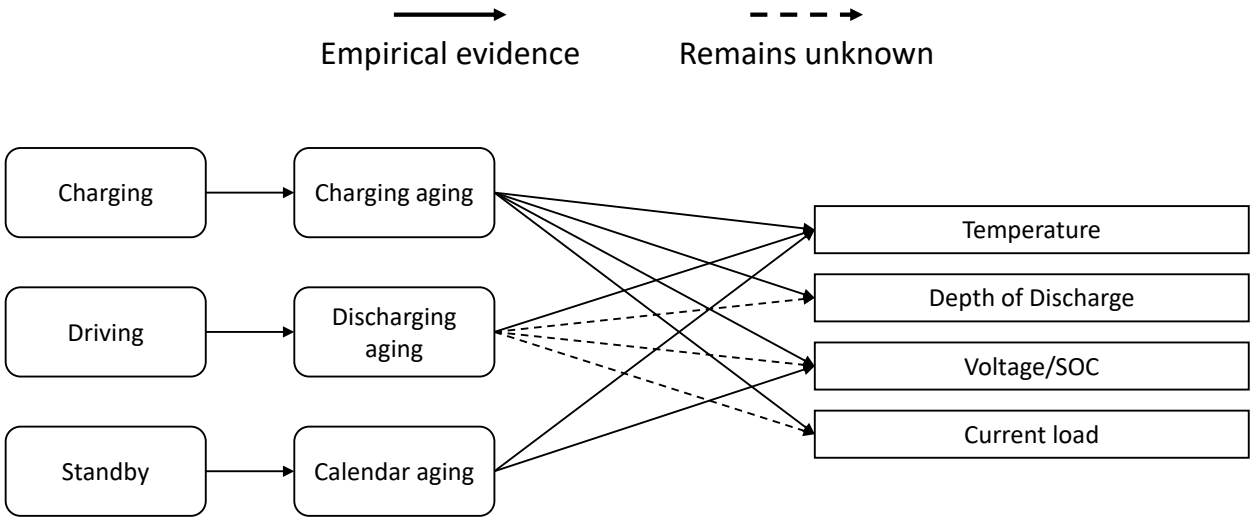

Figure 2. The summary of battery aging based on the use of BEV.

The BMS and ECUs are thought to be the solution to the current EVs' optimized battery life. The research mentioned above demonstrates that the BMS and ECUs are under pressure to act to ensure the vehicle's safety [83,84]. The approach of handing over control of the vehicle to the driver rather than battery optimization is used in most vehicles. The BMS or ECUs would only handle the most extreme circumstances when driving due to the low production cost necessary in the majority of low-end EVs. This is further supported by current studies on the data collected from EVs [89]. Therefore, the discussions on important aging factors are made of the four primary causes—temperature, DOD, voltage and SOC, and current load—as well as the best operating conditions. The summarized reactions to each factor are shown in Figure 3.

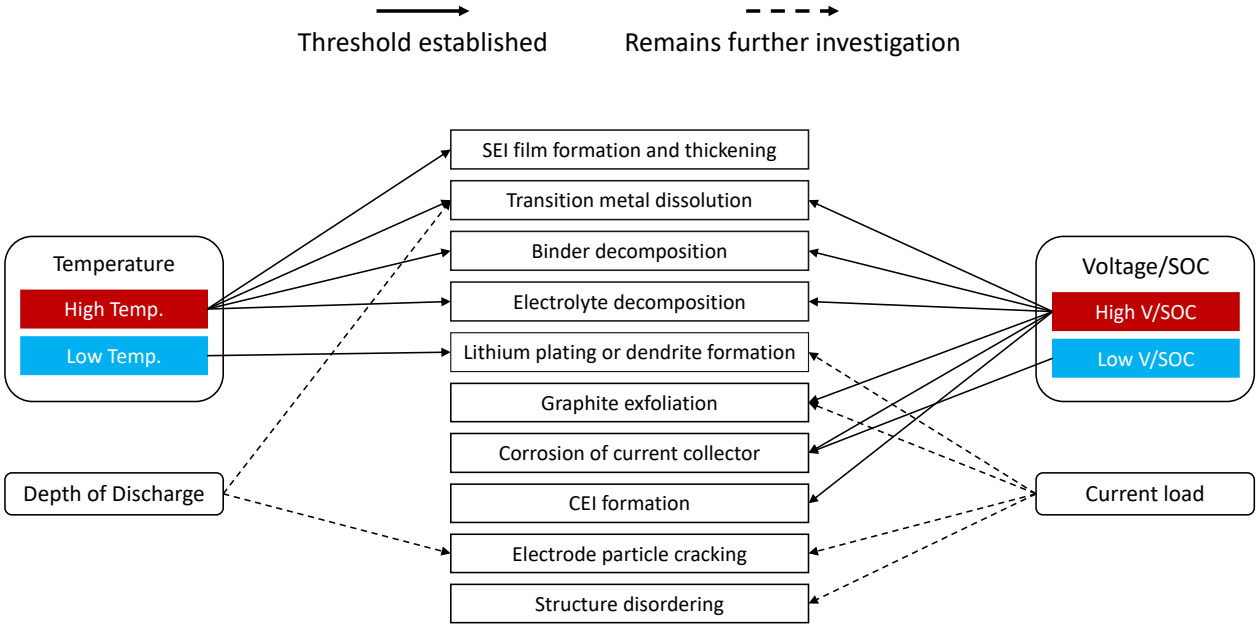

Figure 3. The summary of electrochemical reactions on the driving variables.

3. The Recognition of Driving Behavior

Driving behaviors may be recognized using a range of instruments, such as the inertial measurement unit (IMU), global positioning system (GPS) trajectory, radar, camera, and onboard diagnostics II (OBD-II). The camera technique is not taken into consideration since it raises privacy concerns with biometric data. Currently, there are only two ways to obtain the battery data: via the CAN bus or by performing a terminal charge and discharge test on the battery pack, which necessitates removing the entire battery pack from the EV. This study focuses on CAN bus data, which is the most common technique for making it possible to analyze battery cells. There are conventional and deep learning methods for predicting driving patterns or behaviors using CAN data. The conventional method is based on data analyses using math and statistics. The segments of the driving patterns can be described by a wide range of conventional models, including HMM, GMM, SVM, NB, FL, and KNN. To forecast the desired driving patterns, deep learning models (i.e., RNN, CNN, and fusion models) instead concentrate on decoding the temporal and spatial characteristics.

3.1. The EV Dataset

In order to comprehend the impact of the combination of LiB and EV, better, data-driven approaches hold much promise. A reliable cloud-based architecture is required for the mass production environment in order to gather data and diagnose the data [90]. The following two approaches can be used to collect data to analyze battery life: (1) through the CAN bus; (2) a terminal charge and discharge test on the battery pack, which necessitates the complete battery pack removal from the BEV. Therefore, the data collection using the CAN bus is more feasible for such studies. Additionally, extra real-world driving data are required for fault diagnostics in various scenarios, as well as thermal management and health management [91]. They consist of the calculation of battery aging, distance, end of life (EOL), and remaining useful life (RUL). The real-world EV data contain distinct operations bound to have different fading characteristics compared to lab data and simulations. The driving cycle data (e.g., worldwide harmonized light vehicles test cycles (WLTC) and EURO 6 new European driving cycle (NEDC)) also demonstrated through in-depth investigations of the natural world that various operations and environments on BEVs will significantly impact the battery [92,93]. Therefore, rather than using the constant criteria in

the lab, a precise assessment of the battery health and aging mechanisms can only be made during an actual EV run.

Gonçalo et al. [64] summarized the detailed list of data, including laboratory data, practical driving cycle data, and synthetic data that are frequently used in assisting the BMS. The theoretical basis of the measurements is typically established using lab data (e.g., SOC, SOH). In order to supplement existing data and evaluate the management system under harsh conditions, synthetic data are deployed. To evaluate the performance with the standard in various nations, real-world driving cycle data are required for the EV's final certification. However, the majority of the data only focuses on battery information, and there are few records of driving activities.

Finding data in the most cutting-edge industry takes significant work. Manufacturers are reluctant to provide any details. Yet, the OBD-II interface's data collection process is complicated. The manufacturers have their own protocols to stop rivals and safeguard the vehicles. Using an off-the-shelf IoT reader on the interface is generally impossible. As a result, access to the OBD-II data requires a customized IoT device [65]. Studies have also revealed that in order to examine different driving styles, the battery data sampling range should be between 0.1 and 3 s [46]. To our knowledge, only a few EV datasets shown in Table 4 can meet the requirements of fine-time granularity, driving data integrity, and being labeled and publicly accessible. The following table compiles the prospective data that are available to the general public, and expands the data set to include the EV CAN data from [64]. The features on the datasets are evaluated to ensure that they include at least the high voltage (HV) battery (e.g., voltage, current, temperature, SOC, and SOH) and driving features (e.g., padding operations, speed, throttle, and temperature). The onboard independent or integrated IMU and GPS sensing data may be included, depending on the vehicles and dataset. The partially annotated datasets included below make it possible to construct and analyze the real-world EV immediately since the driving behavior recognition methods mentioned in the following sections are based on their self-simulated data or remain unpublished.

Table 4. The public CAN bus data for driving behavior recognition.

Dataset	Access	No. of Features	Sampling Rate	Battery Info.	Labels
[94]	HCRL	54	1 s	-	Driver
[95]	VED	22	1 s	SOC, A, V	Trip
[96]	Battery and Heat in R.D.C.	28	0.1 s	A, V, C	-
[89]	Nissan Leaf	31	0.25 s	SOC, SOH, A, V, C	Driver and Trip

A: high voltage battery current; V: voltage; C: temperature.

3.2. Conventional Driving Behavior Recognition

The typical approaches to recognizing driving behavior are primarily summarized in this section. The applied statistical, mathematical, and empirical analysis of the driving data provides the foundation for these models. The following methods are discussed based on the CAN bus data: HMM, GMM, SVM, NB, FL, and KNN. Figure 4 summarizes the conventional machine learning methods for driving behavior detection which demonstrated an increase in the accuracy rate from 72.9 to 99.85%.

3.2.1. Hidden Markov Model (HMM)

For low-level or fragmented driving behaviors, the HMM and its derivative approaches showed a simple answer. Using CAN data, the HMM can predict simple driving intents (including left and right turns, stops, lane changes, etc.) with the best performance of 90% accuracy in less than 2 s [9]. Lane change using image detection can be simply accomplished to assess the behavior when a camera is used [10]. The simple HMM is also strengthened by the derived models (hierarchical HMM/multi-layer) to reflect some of the high-level actions [11]. The hierarchical HMM can describe the connections between HMMs in multi-layers [12]. Therefore, multiple HMMs can identify a wide variety of

behaviors. The hierarchical hidden Markov model (HHMM) then calculates the end result after each HMM has described the low-level operations [13]. The disadvantage of the HMM is that further embedding is necessary because the input data do not come straight from the CAN bus. Additionally, it needs to take time sequences into account. Abe et al. [14] suggested that the auto-regressive hidden Markov model (AR-HMM) take the order of the input samples into account and provide the HMM with the sequence information. However, feature extraction, model structure, and temporal segmentation still highly influence the outcomes.

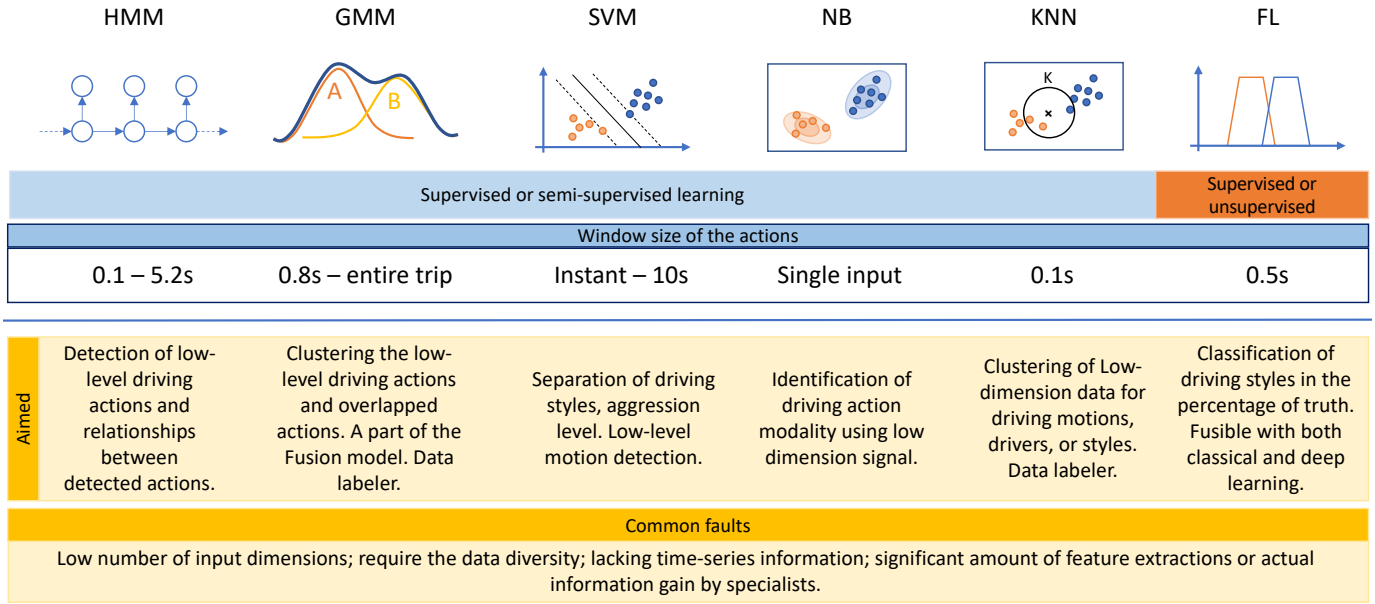

Figure 4. The overview of classical driving behavior detection methods.

3.2.2. Gaussian Mixture Model (GMM)

The goal of this probabilistic model was to increase the data's log-likelihood in Gaussian distributions. The mixture mentioned in relation to the function was made up of several Gaussians. As a generative model, the GMM can handle cluster overlapping, establishing the cluster's non-circular shape. The basic algorithm assigns data points based on probability and is called expectation maximization. K-Means, which classifies data center clusters, is a specific example of a GMM. The cluster would take on a circular shape when measured using Euclidean distance.

When performing behavior analysis, GMMs can pinpoint low-level driving behaviors. For example, pedal operation patterns can be modeled [15]. With a 20 s input and a 10 s stride, Carmona et al. [16] showed how aggressive and non-aggressive motions could be clustered by a GMM. Trips manually tagged the input, and produced the results of 89.21% non-aggressive and 92.65% aggressive. It successfully identified the behavior by only three attributes from the collected data (i.e., mean of throttle, std. of RPM, and the average speed). Shakib et al. [17] employed the maximal information coefficient (MIC) to choose features while extending to the complex input. Multiple models, including GMM, Fuzzy C-means, and K-means, are used to assess the complex input features, with compelling results in each case. Furthermore, Mardi et al. [18] provide a fusion technique using a sophisticated GMM-based model. After performing data preprocessing, feature extraction, and SVM classification, the model employed potential sensing data from a smartwatch to identify the behavior. The fusion model outperformed the GMM in terms of accuracy. In addition to motion patterns, the GMM model can serve as a data labeler [19] for other models. K-means clustering is applied by Song et al. to categorize their data in order to evaluate driver risk in a random forest (RF) model.

3.2.3. Support Vector Machine (SVM)

Another method for resolving issues in the classification of isolated or fragmented behaviors is SVM [20]. By using a single spatiotemporal input, Wang et al. [21] estimate the time-to-collision between two autos using the SVM. To obtain these variables, the input data were preprocessed from the CAN bus data, radar, GPS, and video. Their model has one output and an 80% accuracy rate. There are situations when the SVM's output has many results, with one output compared to the rest of the class [22,23]. With the hybrid framework of SVM with the HMM and a hybrid-state system framework (HSS), Amsalu et al. [24] demonstrate an accuracy rate of 97% on the estimation of the driver's judgments close to the intersection. The SVM model served as a pre-model for the subsequent models. In the studies described, complex feature extraction is still required even though SVM exhibits excellent potential.

SVM accepts semi-supervised input data, similar to the majority of clustering techniques. A semi-supervised support vector machine (S3VM) is used in [25] to determine the level of aggression by throttle opening and vehicle speed. The input movements are first clustered by supervised K-means clustering, which labels the motions in the dataset. When employing the S3VM, it is important to note that the dataset requires precise determination of the number of clusters [26]. The elbow approach should be employed in the appropriate models to test the number of clusters (e.g., SVM, GMM) [27]. It is also possible to test the size of the SVM's data set and the various kernels in order to improve performance [25]. SVM is more important in characterizing low-level motions in driving style analysis. In the era of big data, it can be utilized as an embedding model for high-level models (e.g., decision tree, CNN, HMM). However, the low number of dimensions in the input data, the random labeling by clustering algorithms, and the desire for diversity in the dataset should be considered as some of the SVM's vulnerabilities.

3.2.4. Naive Bayes (NB)

The NB is the most straightforward probability model for identifying driving behavior. The simple model effectively provides a predictor that can be interpreted from the inputs to the driving signals. The conditional probabilities of the driver's action modality (low, medium, or high) can be used to determine the significance of the relevant features (including acceleration, reaction, foot displacement time, etc.) based on the statistical summarizing of low dimensions of variables [28]. These low dimensions signals also have the benefit of making independent activities more explicit. Additionally, Wu et al. [29] note that since some characteristics may overlap in 2D, it is preferable to reveal them in 3D. When diverse compositions of multi-dimensional characteristics are used, features can group driving behaviors by whether they are normal or abnormal. The coordinate data from the accelerometer are particularly well-categorized by the Bayesian model. When the variation, std., mean, duration, max, and orientation are considered, Chen et al. [30] show that the Bayesian model outperforms the SVM. Requiring a significant number of feature extractions by hand or specialists is the NB's flaw. The size and variety of the dataset are important factors for examining correlations in the features.

3.2.5. Fuzzy Logic (FL)

The accurate estimation in categorizing driving behavior was demonstrated using FL and its derivatives (HMM, C-mean, deep learning). In the FL approach, the vague classification can be easily modeled based on some if-then rules. For the prediction in the FL approach, much research specifies various sets of rules or problems related to the driving behaviors (e.g., steering angle, velocity, acceleration) [31–33]. In many situations, driving behaviors do not necessarily belong to the signal class (e.g., aggressive or non-aggressive) [34]. FL enables the classifications to contain a certain amount of truth (e.g., 30% aggressive and 70% non-aggressive). By interpolating the actions and rules with imprecise linguistic definitions, fuzzy inference also clarifies the driving behaviors from the data.

Fernández and Ito [33] provide an example of driver classification based on aggressive and passive driving styles. The functions of the accelerator, brake, and speed are established as the rules to categorize the driving profiles in the fuzzification interface. The frequency of pedal use (i.e., the percentage of times the rules were taken into account) is specified in the inference system. The criteria used to define the aggressive and passive profiles serve as the foundation for the defuzzification interface. This defuzzification result is then used to assign the driver to a certain profile.

An FL-based fusion model enhances the capabilities to create a sophisticated prediction system. With the FL-HMM, Deng and Söffke [32] improve the prediction of driving behavior and enable the recognition of scenes (e.g., highways and nearby vehicles) and operations (e.g., steering wheel angle, acceleration, and braking). To anticipate the driver's risky behaviors, Li et al. [35] create a fuzzy-macro long short-term memory (LSTM). The method computes the unsafe level using the number of abrupt accelerations, braking, and average speed per 100 km. The deep learning models (i.e., multilayer perceptron (MLP), CNN, and LSTM) are examined to enable the preservation of the temporal signal. Furthermore, FL can function effectively in IMU sensors such as magnetometers, gyroscopes, and accelerometers [36].

The requirement that definitions be based on actual information gained from the experience of experts is one of the shortcomings of FL. The feature thresholds are determined by prior information. Field expertise is required to pinpoint the precise characteristics that have an impact on the associated maneuvers. In order to resolve the threshold problem, The borders of a specific feature can be clustered out using supervised learning techniques (i.e., NB and SVM).

3.2.6. K-Nearest Neighbour (KNN)

KNN is a widely used non-parametric machine learning method for regression and classification [37]. Model definition or training are not required to be preset. Compared to the others, KNN is simple to use and comprehend. In order to identify between 50 drivers on a particular road, Li et al. [20] created KNN classifiers. The average and standard deviation for each vehicle's characteristics, including speed, acceleration, the position of the brake and gas pedals, steering angle, and lateral position, are calculated. When compared to an SVM and an artificial neural network (ANN), the accuracy only drops by 2% and 6%, respectively. Karri et al. [38] classify the driving behaviors of drivers at traffic intersections with traffic lights using CAN data from the driving simulator. By including the CAN characteristics (i.e., throttle and braking pedal), the accuracy is 92.3% and 90.1% during training and testing. In the meantime, KNN can work in tandem with other ML methods including Bayesian, SVM, and K-means to boost clustering performance [39]. The KNN's parameter K and high computational cost are its drawbacks. It is necessary to test the K value and even implement the automatic K search [40].

3.3. Deep Learning Driving Behavior Recognition

Driving identification using deep learning produced highly accurate results compared to traditional approaches. This is due to the time series data from the CAN bus that can be used with a variety of techniques (i.e., RNN, CNN, and fusion models). It also increases the preprocessing steps before entering the CAN data into the models. These preparation procedures include trip and time step segmentation on the multi-dimensional time series data as well as abnormal data filtering, normalization, and preprocessing for abnormal data. The mainstream RNN, CNN, and fusion models used in deep learning are covered in the subsequent sections. Figure 5 below illustrates the deep learning approach's full workflow.

3.3.1. Recurrent Neural Network (RNN)

An RNN is a form of neural network that uses cycle connections between nodes to trace the input's antecedent. An RNN takes into account the input sequence, in contrast to an ANN. Given that the driving actions are not independent in pure distribution but rather

temporally connected, this is similar to driving patterns. Therefore, the LSTM, a variation of RNN, showed an accurate classification rate for driving behaviors when applying the data from the IMU and GPS [49–51]. In fact, the RNN forecasts anything in the BEV-related indicators. The temperature of the Li-ion battery is predicted accurately by the BEV time series motions. Jiang et al. [52] successfully estimated the surface temperature with a maximum absolute error of 0.75 °C using the LSTM method and gated recurrent unit (GRU). The Li-ion SOC for the BMS is predicted by Khalid et al. [53] with an RMSE of 1.527%. References [54–56] demonstrate the data-driven methodology for SOH prediction using data on the voltage and current from Li-ion batteries. In spite of this, references [57,58] depict the RUL prediction on the Li-ion battery.

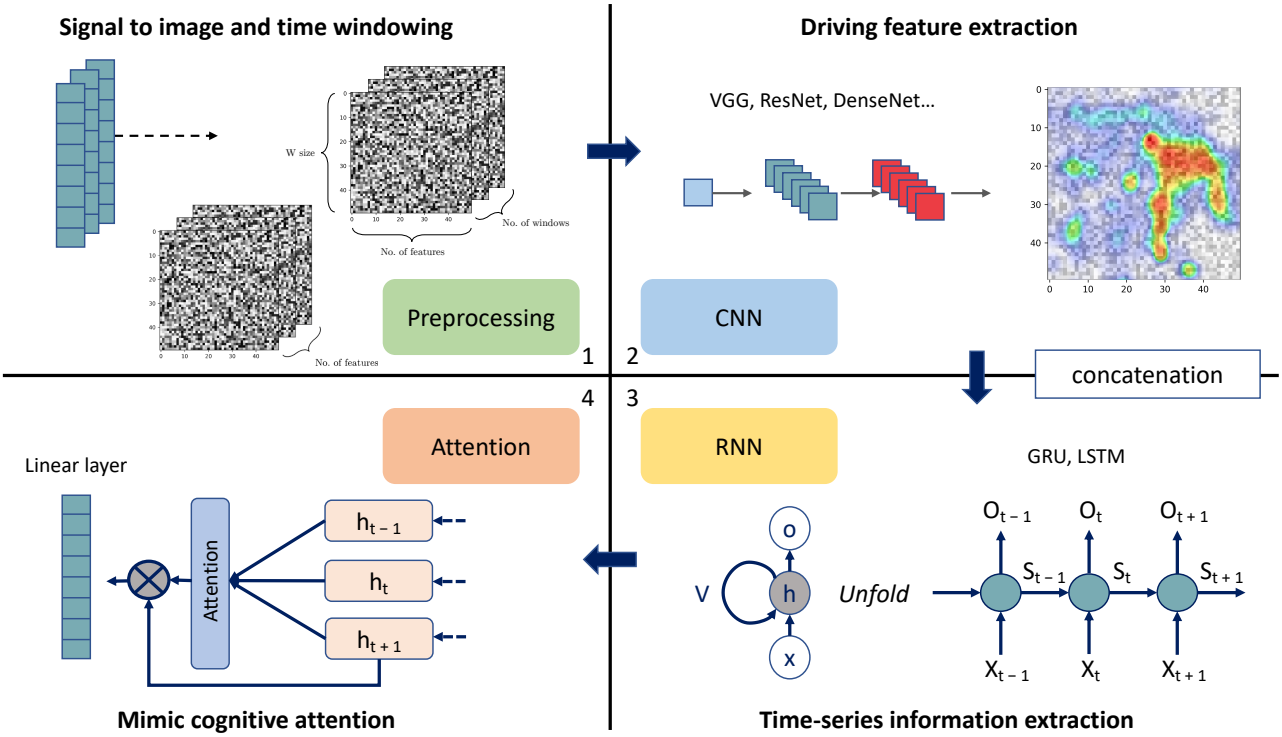

Figure 5. The overview of the deep learning approach in driving behavior detection. 1. data is transformed into an image or nonlinear picture using the RP formula; 2. extracted features can be seen by activation heat map; 3. CNN results are concatenated or directly input into RNN models; and 4, attention mechanisms are used after RNN for classifications.

The RNN may also instantaneously offer relevant responses or suggestions to assist with driving. An LSTM is created by Zeng et al. [59] to measure the level of comfort while riding using three inputs: velocity, longitudinal acceleration, and yaw rate. The data are initially divided into the designated zones, with the peak period and traffic flow taken into account as the input for the LSTM neural network. The LSTM network may then offer driving assistance through real-time suggestions. Similarly, Xing et al. [60] have presented an advanced stacked LSTM model to forecast the energy consumption from the acceleration and deceleration characteristics. They discover that the crucial markers were the frequency and duration of the acceleration and deceleration tendencies. Thus, using LSTM models, safety motion prediction based on trajectories can be accomplished. In the above investigations, the crucial model creation is moved to the preprocessing phases. It is vital to formulate the input based on the objectives. These techniques, which directly impact the model's accuracy rate, include data resampling, segmentation, cyclical encoding, and data windowing [97].

3.3.2. Convolutional Neural Network (CNN)

In the domain of computer vision, the CNN gave a strong performance [41]. When the time-series data were applied to the CNN, it primarily served two purposes: (1) the spatial information attainment for the model, and (2) features extraction and visualization for the input data.

When analyzing CAN bus data for behavior detection, CNN performs the best as a single model recognition. According to Azadani and Boukerche, the CNN model even outperformed the deep convolutional LSTM model in terms of accuracy rate for recognizing driving behavior, with scores of 96.85% and 95.06%, respectively, [42]. They start by looking at the correlation between the data and then extract several key aspects (e.g., fuel consumption, the accelerator, torque, friction, etc.) as the input data. In order to enable the convolutional computation of the time-series data, the input data is then transformed into the image metric structure. Based on a sample rate of 0.1 s, the window is set to 100 s and the stride to 50 s to record the action sequence. The characteristics are viewed as channels or dimensions. The driving behaviors are then determined using two convolutional computations and max-pooling by this end-to-end model.

In behavior identification and visualization, CNN also serves as a feature extractor. One of the crucial phases in the identification of numerous behaviors is feature extraction. In [43], a CNN in the human activity recognition domain is able to capture the local dependency and scale invariance of a signal without domain knowledge of human activity recognition. Local dependence in image identification tasks refers to the closely spaced pixels that are often more interconnected. Because the picture is scale-invariant [44], the task's outcome is unaffected by the image's size. These characteristics are passed on as the CNN applies the recognition of driving behavior. For instance, the data may be created as a time series image and the association between each time can be easily extracted. Furthermore, the scale of the time window and features will not impact the result significantly.

Shahverdy et al. [45] transform the driving signal (i.e., gravity, acceleration, revolutions per minute (RPM), speed, and throttle) from OBD to a 50 × 50 gray-scale image via Pyts recurrence plot [98] for CNN recognition, in order to activate the feature extraction on driving data. The typical driver's response time ranges from 0.7 to 3 s [46]. They provide various time windows for each kind of action. The aggressive detection window has a 50% overlap and a 20 s setting. They create the 50 × 50 pixel image using a 50 ms time window with a 98% overlap for each defined behavior. As the input to the CNN model, all the characteristics are ultimately combined into a single picture (i.e., 150 × 50 pixels). With a complexity of 0.041 million floating-point operations per second (MFLOPS), their method targets the low computational cost of the ECUs and achieves an accuracy rate of 99.76%.

In [47], a fantastic use of driving behavior recognition is shown. The method identifies the driver behavior by using the 32 Hz sample rate data, which contain individual steering behaviors. They implemented the convolutional layer at the start of the residual network, followed by the fully connected (FC) layer and softmax function at the output. Each driver is correctly identified using this technique. The methodology is identical when using this method to identify driving styles, except for the distance comparison features. A difference threshold can be set to detect the aggressive level of the CAN data.

The heat map method may also be used to show the CNN model feature [48,99]. It is possible to see the feature representation of the network inside the picture dimension by applying the global average or max pooling before the FC layer. This is accomplished through class activation mapping, which can be regarded as the reverse procedure on a weighted sum of data in the final convolutional layer to produce the output. The procedure is then reversed to produce the class activation maps using the weighted sum by mapping the anticipated class score back to the previous convolutional layer.

CNN showed a great degree of flexibility in tasks involving the detection of driving behavior. The advantage is the extraction of the temporal and spatial characteristics. It can serve as the unitary feature extraction layer for different learning techniques (e.g., RNN,

residual networks). Nevertheless, the CNN model lacks time series data, in comparison to the RNN models that will be covered in the subsequent section discussing fusion models.

3.3.3. Fusion Models

Fusion models for deep learning address the last major flaw in the recognition of driving behavior. They start by addressing the time series connections between each sample. Zhang et al. [61] showed how to recognize anomalous driving behavior using a basic fusion architecture. The CNN has a direct connection to the bidirectional gated recurrent unit (BiGRU) and has implemented the rectified linear unit (ReLu) and softmax FC layer to categorize the behavior in the 3 s action segment. Their method obtained the best accuracy rate of 98.99% in 3-fold cross-validation using the safety pilot model deployment (SPMD) dataset. A similar end-to-end attention-based fusion model is also demonstrated in [62,63], which are the deep convolutional RNN models. The attention mechanism concentrates on the units of driving behaviors from the collected spatial–temporal activities rather than the intricate sequences of motor motions. Their method's fundamental working principle is to sequentially link the following deep learning units: (1) CNN, (2) RNN, (3) attention unit, and (4) classifier. To link the convolutional output to the RNN input, an FC layer is positioned between the CNN and RNN. Their fusion model surpasses the state-of-the-art solutions (e.g., deep neural network (DNN), LSTM, CNN, decision tree, etc.). The best accuracy rate of 99.78% was attained by the deep convolutional GRU model in [62] when the time window was set to 60 samples with a shift of 6 samples. An accuracy rate of 95.85% is likewise displayed in [63] when training is conducted only using IMU sensing data.

Table 5 provides a list of the standard recognition methods used in both deep learning and classical machine learning. The recognition level and accuracy of the methods are clarified in each of the categories, which provide the blueprint for the detection of vehicle usage. When compared to deep learning, traditional machine learning exhibits lower accuracy and a lower level of identification of the driving activity. Deep learning, on the other hand, predicts driving behavior at a higher level with incredibly high accuracy but with less clarity. Therefore, several driving patterns can be discovered to explain the reason for accelerated aging depending on the intended correlation of battery aging metrics. Moreover, the lifetime driving activity mixture can be detected for subsequent linkage with the SOH on the EV battery.

Table 5. Comparison of conventional and deep learning recognition.

Category	Methods	Used Features	Recognition Level	Data Window	Accuracy
HMM	HMM [9]	Steering, gas, and brake *	Driving action	0.3–5.2 s	82–90%
	HHMM [12]	CAN data *	Sequence of driving state	2–5.5 s	93–99.85%
	AR-HMM [14]	Speed, pedal stroke *	Driving state	0.1 s	-
GMM	GMM [15,16]	Following distance, all CAN data, GPS *,†	Driving action	0.8–20 s	72.9–92.65%
	GMM-Fusion [18]	IMU *	Driving action, sequence of driving action	Entire trip	-
SVM	SVM [21]	Radar, video, GPS, CAN data †	Single event	10 s	80.8%
	SVM-hybird [24]	CAN data, GPS †	Driving action	0.1 s	97%
	S3VM [26]	Steering, acceleration, brake, gear *	Driving style	instant	86.6%
FL	FL-variant [36]	IMU †	Driving style	0.5 s	92%
KNN	KNN [38]	Brake, GPS, throttle, traffic light *	Single event	0.1s	90.1%
RNN	LSTM [50]	IMU, CAN data *	Driver identification	30 s	74.7–82.3%
	Stacked-LSTM [49,51]	IMU, GPS, camera *,†	Driving style	6.4 s	86–96%
CNN	CNN [42]	CAN data †	Driver identification	100 s	96.85%
	CNN image transform [45]	CAN data †	Driving style	20 s	83.8–99%
Fusion	CNN-LSTM-Attention [63]	IMU, GPS †	Driving action and state	1 s	95.85%
	CNN-RNN-Attention [62]	CAN data †	Driver identification	60 s	97–98.4%
	CNN-BiGRU [61]	CAN data, GPS, Driver †	Driving style	3 s	97.33%

* Simulated data. † Real vehicle collected data. Driving action: non-stop straight road, stop, left turn, right turn, etc. Driving state: stop, acceleration, coasting, braking, etc. Driving style: normal, aggressive, passive, etc.

4. Summaries and Prospects

In conclusion, this paper summarized the Li-ion battery degradation and the driving behavior aimed at SOH analysis to prolong the battery life in real-world EV applications. To keep the battery in the ideal SOH, the advanced BMS should also retain the four main SOH aging factors, including temperature, DOD, voltage, and SOC, and current load. The temperature is one of the factors affected by the driving operation, which is being proven so far in the lab and real-world driving tests. To bridge the gap, this work reviewed the different driving behavior recognition methods that are intended to rebuild the entire driving process for the analysis for the rest of the aging factors. The distribution and sequence of the action and state of a driving trip can be obtained by utilizing classic machine learning. At the same time, deep learning methods can classify the driver, driving style, and driving state in a particular trip. As a result, the SOH aging factors can be defined clearly by linking its electrochemical characteristics to the usage of the EV instead of the ambiguous driving style, which is simply defined as aggressive or normal. Although the majority of driving behavior identification research is based on ICE cars, few real-world EV driving datasets are also provided for the implementation, identification, or enhancement of driving behavior recognition in EV applications.

Just a small number of studies, to our knowledge, have linked battery aging to the lifespan operation of EVs, and yet this is a promising approach to an open challenge that involves the entire BEV industry. Even though some of the BEV models have not met the 10 year EOL industry norm, which is necessary to allow for data-driven analysis in a real-world setting, our work can recognize the driving behavior from the data provided. This, along with further analysis in simulation, paves the way to a better understanding of SOH estimation.

Author Contributions: Conceptualization, K.S.C.; battery review, K.S.C.; driving behavior review, K.S.C.; EV data review, K.S.C.; formal analysis, K.S.C.; investigation, K.S.C.; resource, R.T., S.-K.T. and G.P.; writing—original draft preparation, K.S.C.; writing—review and editing, K.S.C., K.L.W., D.A., R.T., S.-K.T. and G.P.; supervision, R.T., S.-K.T. and G.P.; project administration, R.T., S.-K.T., and G.P. All authors have read and agreed to the published version of the manuscript.

Funding: This research received no external funding.

Institutional Review Board Statement: Not applicable.

Informed Consent Statement: Not applicable.

Data Availability Statement: Not applicable.

Acknowledgments: This work was supported in part by the Macao Polytechnic University - Edge Sensing and Computing: Enabling Human-centric (Sustainable) Smart Cities (RP/ESCA-01/2020) and by the H2020 project titled "European Bus Rapid Transit of 2030: Electrified, Automated, Connected" EBRT-Grant Agreement N. 101095882.

Conflicts of Interest: The authors declare no conflict of interest.

References

1. Wang, Y.; Yu, Y.; Huang, K.; Tang, B. From the Perspective of Battery Production: Energy–Environment–Economy (3E) Analysis of Lithium-Ion Batteries in China. *Sustainability* **2019**, *11*, 6941. [CrossRef]
2. Guo, J.; Li, Y.; Pedersen, K.; Stroe, D.I. Lithium-Ion Battery Operation, Degradation, and Aging Mechanism in Electric Vehicles: An Overview. *Energies* **2021**, *14*, 5220. [CrossRef]
3. Yao, L.; Xu, S.; Tang, A.; Zhou, F.; Hou, J.; Xiao, Y.; Fu, Z. A review of lithium-ion battery state of health estimation and prediction methods. *World Electr. Veh. J.* **2021**, *12*, 113. [CrossRef]
4. How, D.N.; Hannan, M.; Lipu, M.H.; Ker, P.J. State of charge estimation for lithium-ion batteries using model-based and data-driven methods: A review. *IEEE Access* **2019**, *7*, 136116–136136. [CrossRef]
5. Noura, N.; Boulon, L.; Jemeï, S. A Review of Battery State of Health Estimation Methods: Hybrid Electric Vehicle Challenges. *World Electr. Veh. J.* **2020**, *11*, 66. [CrossRef]
6. Wang, H.; Wang, X.; Han, J.; Xiang, H.; Li, H.; Zhang, Y.; Li, S. A Recognition Method of Aggressive Driving Behavior Based on Ensemble Learning. *Sensors* **2022**, *22*, 644. [CrossRef]

7. Xu, W.; Wang, J.; Fu, T.; Gong, H.; Sobhani, A. Aggressive driving behavior prediction considering driver's intention based on multivariate-temporal feature data. *Accid. Anal. Prev.* **2022**, *164*, 106477. [CrossRef]
8. Lee, K.W.; Yoon, H.S.; Song, J.M.; Park, K.R. Convolutional neural network-based classification of driver's emotion during aggressive and smooth driving using multi-modal camera sensors. *Sensors* **2018**, *18*, 957. [CrossRef]
9. Tran, D.; Sheng, W.; Liu, L.; Liu, M. A Hidden Markov Model based driver intention prediction system. In Proceedings of the 2015 IEEE International Conference on Cyber Technology in Automation, Control, and Intelligent Systems (CYBER), Shenyang, China, 8–12 June 2015; pp. 115–120.
10. Liu, P.; Kurt, A.; Özgüner, Ü. Trajectory prediction of a lane changing vehicle based on driver behavior estimation and classification. In Proceedings of the 17th international IEEE Conference on Intelligent Transportation Systems (ITSC), Qingdao, China, 8–11 October 2014; pp. 942–947.
11. Fine, S.; Singer, Y.; Tishby, N. The hierarchical hidden Markov model: Analysis and applications. *Mach. Learn.* **1998**, *32*, 41–62. [CrossRef]
12. He, L.; Zong, C.f.; Wang, C. Driving intention recognition and behaviour prediction based on a double-layer hidden Markov model. *J. Zhejiang Univ. Sci. C* **2012**, *13*, 208–217. [CrossRef]
13. Zhu, T.; Khajepour, A.; Zong, C.; Mai, L.; Deng, H. Driving condition identification based on HHMM model–Application to the simulation of heavy duty vehicle. In *The Dynamics of Vehicles on Roads and Tracks*; CRC Press: Boca Raton, FL, USA, 2016; pp. 670–675.
14. Abe, K.; Miyatake, H.; Oguri, K. A study on switching AR-HMM driving behavior model depending on driver's states. In Proceedings of the 2007 IEEE Intelligent Transportation Systems Conference, Bellevue, WA, USA, 30 September–3 October 2007; pp. 806–811.
15. Miyajima, C.; Nishiwaki, Y.; Ozawa, K.; Wakita, T.; Itou, K.; Takeda, K.; Itakura, F. Driver modeling based on driving behavior and its evaluation in driver identification. *Proc. IEEE* **2007**, *95*, 427–437. [CrossRef]
16. Carmona, J.; Miguel, M.A.D.; Martin, D.; Garcia, F.; Escalera, A.D.L. Embedded System for Driver Behavior Analysis Based on GMM. In Proceedings of the 2016 IEEE Intelligent Vehicles Symposium (IV), Gothenburg, Sweden, 19–22 June 2016; Institute of Electrical and Electronics Engineers Inc.: New York, NY, USA, 2016; Volume 8, pp. 61–65. . [CrossRef]
17. Shakib, M.N.; Shamim, M.; Shawon, M.N.H.; Isha, M.K.F.; Hashem, M.M.; Kamal, M.A. An Adaptive System for Detecting Driving Abnormality of Individual Drivers Using Gaussian Mixture Model. In Proceedings of the 2021 5th International Conference on Electrical Engineering and Information Communication Technology (ICEEICT), Dhaka, Bangladesh, 18–20 November 2021; Institute of Electrical and Electronics Engineers Inc.: New York, NY, USA, 2021. [CrossRef]
18. Putri, R.R.M.; Yang, C.H.; Chang, C.C.; Liang, D. Smartwatch-Based Open-Set Driver Identification by Using GMM-Based Behavior Modeling Approach. *IEEE Sens. J.* **2021**, *21*, 4918–4926. [CrossRef]
19. Song, X.; Yin, Y.; Cao, H.; Zhao, S.; Li, M.; Yi, B. The mediating effect of driver characteristics on risky driving behaviors moderated by gender, and the classification model of driver's driving risk. *Accid. Anal. Prev.* **2021**, *153*, 106038. [CrossRef] [PubMed]
20. Li, Z.; Zhang, Q.; Zhao, X. Performance analysis of K-nearest neighbor, support vector machine, and artificial neural network classifiers for driver drowsiness detection with different road geometries. *Int. J. Distrib. Sens. Netw.* **2017**, *13*. [CrossRef]
21. Wang, H.; Gu, M.; Wu, S.; Wang, C. A driver's car-following behavior prediction model based on multi-sensors data. *Eurasip J. Wirel. Commun. Netw.* **2020**, *2020*, 10. [CrossRef]
22. Abe, S. Analysis of multiclass support vector machines. *Thyroid* **2003**, *21*, 3772.
23. Bin, Z.; Yong, L.; Shao-Wei, X. Support vector machine and its application in handwritten numeral recognition. In Proceedings of the Proceedings 15th International Conference on Pattern Recognition, ICPR-2000, Barcelona, Spain, 3–7 September 2000; Volume 2, pp. 720–723.
24. Amsalu, S.B.; Homaifar, A.; Afghah, F.; Ramyar, S.; Kurt, A. Driver behavior modeling near intersections using support vector machines based on statistical feature extraction. In Proceedings of the 2015 IEEE Intelligent Vehicles Symposium (IV), Seoul, Republic of Korea, 28 June–1 July 2015; Institute of Electrical and Electronics Engineers Inc.: New York, NY, USA, 2015; Volume 8, pp. 1270–1275. [CrossRef]
25. Yang, K.; Haddad, C.A.; Yannis, G.; Antoniou, C. Driving behavior safety levels: Classification and evaluation. In Proceedings of the 2021 7th International Conference on Models and Technologies for Intelligent Transportation Systems (MT-ITS), Heraklion, Greece, 16–17 June 2021; Institute of Electrical and Electronics Engineers Inc.: New York, NY, USA, 2021; Volume 6. [CrossRef]
26. Wang, W.; Xi, J.; Chong, A.; Li, L. Driving Style Classification Using a Semisupervised Support Vector Machine. *IEEE Trans. Hum.-Mach. Syst.* **2017**, *47*, 650–660. [CrossRef]
27. Syakur, M.; Khotimah, B.; Rochman, E.; Satoto, B.D. Integration k-means clustering method and elbow method for identification of the best customer profile cluster. *Proc. IOP Conf. Ser. Mater. Sci. Eng.* **2018**, *336*, 012017. [CrossRef]
28. Bouslimi, W.; Kassaagi, M.; Lourdeaux, D.; Fuchs, P. Augmented Naïve Bayesian network for driver behavior modeling. In Proceedings of the IEEE Proceedings. Intelligent Vehicles Symposium, Las Vegas, NV, USA, 6–8 June 2005; Volume 2005, pp. 236–242. [CrossRef]
29. Wu, X.; Zhou, J.; An, J.; Yang, Y. Abnormal driving behavior detection for bus based on the Bayesian classifier. In Proceedings of the 2018 Tenth International Conference on Advanced Computational Intelligence (ICACI), Xiamen, China, 29–31 March 2018; Institute of Electrical and Electronics Engineers Inc.: New York, NY, USA, 2018; Volume 6, pp. 266–272. [CrossRef]

30. Chen, Z.; Yu, J.; Zhu, Y.; Chen, Y.; Li, M. D3: Abnormal driving behaviors detection and identification using smartphone sensors. In Proceedings of the 2015 12th Annual IEEE International Conference on Sensing, Communication, and Networking (SECON), Seattle, WA, USA, 22–25 June 2015; pp. 524–532.
31. Tang, J.; Liu, F.; Zhang, W.; Ke, R.; Zou, Y. Lane-changes prediction based on adaptive fuzzy neural network. *Expert Syst. Appl.* **2018**, *91*, 452–463. [CrossRef]
32. Deng, Q.; Söffker, D. Improved driving behaviors prediction based on fuzzy logic-hidden markov model (fl-hmm). In Proceedings of the 2018 IEEE Intelligent Vehicles Symposium (IV), Changshu, China, 26–30 June 2018; pp. 2003–2008.
33. Fernandez, S.; Ito, T. Driver classification for intelligent transportation systems using fuzzy logic. In Proceedings of the 2016 IEEE 19th International Conference on Intelligent Transportation Systems (ITSC), Rio de Janeiro, Brazil, 1–4 November 2016; Institute of Electrical and Electronics Engineers Inc.: New York, NY, USA, 2016; Volume 12, pp. 1212–1216. [CrossRef]
34. Quintero, M.C.G.; López, J.O.; Pinilla, A.C.C. Driver behavior classification model based on an intelligent driving diagnosis system. In Proceedings of the 2012 15th International IEEE Conference on Intelligent Transportation Systems, Anchorage, AK, USA, 16–19 September 2012; pp. 894–899.
35. Li, D.C.; Lin, M.Y.C.; Chou, L.D. Macroscopic Big Data Analysis and Prediction of Driving Behavior with an Adaptive Fuzzy Recurrent Neural Network on the Internet of Vehicles. *IEEE Access* **2022**, *10*, 47881–47895. [CrossRef]
36. Eftekhari, H.R.; Ghatee, M. Hybrid of discrete wavelet transform and adaptive neuro fuzzy inference system for overall driving behavior recognition. *Transp. Res. Part F Traffic Psychol. Behav.* **2018**, *58*, 782–796. [CrossRef]
37. Cunningham, P.; Delany, S.J. k-Nearest neighbour classifiers-A Tutorial. *ACM Comput. Surv. (CSUR)* **2021**, *54*, 1–25. [CrossRef]
38. Karri, S.L.; Silva, L.C.D.; Lai, D.T.C.; Yong, S.Y. Classification and Prediction of Driving Behaviour at a Traffic Intersection Using SVM and KNN. *SN Comput. Sci.* **2021**, *2*, 209. [CrossRef]
39. Taunk, K.; De, S.; Verma, S.; Swetapadma, A. A brief review of nearest neighbor algorithm for learning and classification. In Proceedings of the 2019 International Conference on Intelligent Computing and Control Systems (ICCS), Madurai, India, 15–17 May 2019; pp. 1255–1260.
40. Zhang, S.; Li, X.; Zong, M.; Zhu, X.; Cheng, D. Learning k for knn classification. *ACM Trans. Intell. Syst. Technol.* **2017**, *8*, 1–19. [CrossRef]
41. Krizhevsky, A.; Sutskever, I.; Hinton, G.E. ImageNet classification with deep convolutional neural networks. *Commun. ACM* **2017**, *60*, 84–90. [CrossRef]
42. Azadani, M.N.; Boukerche, A. Performance evaluation of driving behavior identification models through can-bus data. In Proceedings of the 2020 IEEE Wireless Communications and Networking Conference (WCNC), Seoul, Republic of Korea, 25–28 May 2020; pp. 1–6.
43. Zeng, M.; Nguyen, L.T.; Yu, B.; Mengshoel, O.J.; Zhu, J.; Wu, P.; Zhang, J. Convolutional Neural Networks for human activity recognition using mobile sensors. In Proceedings of the 6th International Conference on Mobile Computing, Applications and Services, Austin, TX, USA, 6–7 November 2014; Institute of Electrical and Electronics Engineers Inc.: New York, NY, USA, 2015; Volume 1, pp. 197–205. [CrossRef]
44. Singh, B.; Davis, L.S. An Analysis of Scale Invariance in Object Detection—SNIP. *arXiv* **2017**, arXiv:1711.08189.
45. Shahverdy, M.; Fathy, M.; Berangi, R.; Sabokrou, M. Driver behavior detection and classification using deep convolutional neural networks. *Expert Syst. Appl.* **2020**, *149*, 113240. [CrossRef]
46. McGehee, D.V.; Mazzae, E.N.; Baldwin, G.S. Driver reaction time in crash avoidance research: Validation of a driving simulator study on a test track. In *Proceedings of the Human Factors and Ergonomics Society Annual Meeting*; Sage Publications Sage CA: Los Angeles, CA, USA, 2000; Volume 44, pp. 3–320.
47. Azadani, M.N.; Boukerche, A. Siamese temporal convolutional networks for driver identification using driver steering behavior analysis. *IEEE Trans. Intell. Transp. Syst.* **2022**, *23*, 18076–18087. [CrossRef]
48. Selvaraju, R.R.; Cogswell, M.; Das, A.; Vedantam, R.; Parikh, D.; Batra, D. Grad-CAM: Visual Explanations from Deep Networks via Gradient-based Localization. *Int. J. Comput. Vis.* **2020**, *128*, 336–359 . [CrossRef]
49. Kadri, N.; Ellouze, A.; Ksantini, M.; Turki, S.H. New LSTM Deep Learning Algorithm for Driving Behavior Classification. *Cybern. Syst.* **2022**, *54*, 387–405. [CrossRef]
50. Mumcuoglu, M.E.; Alcan, G.; Unel, M.; Cicek, O.; Mutluergil, M.; Yilmaz, M.; Koprubasi, K. Driving behavior classification using long short term memory networks. In Proceedings of the 2019 AEIT International Conference of Electrical and Electronic Technologies for Automotive (AEIT AUTOMOTIVE), Turin, Italy, 2–4 July 2019; pp. 1–6.
51. Saleh, K.; Hossny, M.; Nahavandi, S. Driving behavior classification based on sensor data fusion using LSTM recurrent neural networks. In Proceedings of the 2017 IEEE 20th International Conference on Intelligent Transportation Systems (ITSC), Yokohama, Japan, 16–19 October 2017; pp. 1–6.
52. Jiang, Y.H.; Yu, Y.F.; Huang, J.Q.; Cai, W.W.; Marco, J. Li-ion battery temperature estimation based on recurrent neural networks. *Sci. China Technol. Sci.* **2021**, *64*, 1335–1344. [CrossRef]
53. Khalid, A.; Sundararajan, A.; Acharya, I.; Sarwat, A.I. Prediction of li-ion battery state of charge using multilayer perceptron and long short-term memory models. In Proceedings of the 2019 IEEE Transportation Electrification Conference and Expo (ITEC), Detroit, MI, USA, 19–21 June 2019; pp. 1–6.
54. Sun, H.; Yang, D.; Du, J.; Li, P.; Wang, K. Prediction of Li-ion battery state of health based on data-driven algorithm. *Energy Rep.* **2022**, *8*, 442–449. [CrossRef]

55. Lin, J.; Yan, G.; Wang, C. Li-ion battery state of health prediction based on long short-term memory recurrent neural network. *J. Phys. Conf. Ser.* **2010**, *2010*, 012133. [CrossRef]
56. Yayan, U.; Arslan, A.T.; Yucel, H. A novel method for SoH prediction of batteries based on stacked LSTM with quick charge data. *Appl. Artif. Intell.* **2021**, *35*, 421–439. [CrossRef]
57. Zhang, Y.; Xiong, R.; He, H.; Liu, Z. A LSTM-RNN method for the lithuim-ion battery remaining useful life prediction. In Proceedings of the 2017 Prognostics and System Health Management Conference (PHM-Harbin), Harbin, China, 9–12 July 2017; pp. 1–4.
58. Wang, Z.; Liu, N.; Guo, Y. Adaptive sliding window LSTM NN based RUL prediction for lithium-ion batteries integrating LTSA feature reconstruction. *Neurocomputing* **2021**, *466*, 178–189. [CrossRef]
59. Zeng, L.; Zhang, H.; Han, Q.; Tang, Y.; Ye, L.; Wu, Y.; Zu, H. An LSTM-based driving operation suggestion method for riding comfort-oriented critical zone. *J. Ambient. Intell. Humaniz. Comput.* **2023**, *14*, 755–771. [CrossRef]
60. Xing, Y.; Lv, C.; Mo, X.; Hu, Z.; Huang, C.; Hang, P. Toward Safe and Smart Mobility: Energy-Aware Deep Learning for Driving Behavior Analysis and Prediction of Connected Vehicles. *IEEE Trans. Intell. Transp. Syst.* **2021**, *22*, 4267–4280. [CrossRef]
61. Zhang, Y.; He, Y.; Zhang, L. Recognition method of abnormal driving behavior using the bidirectional gated recurrent unit and convolutional neural network. *Phys. A Stat. Mech. Its Appl.* **2023**, *609*, 128317. [CrossRef]
62. Zhang, J.; Wu, Z.C.; Li, F.; Xie, C.; Ren, T.; Chen, J.; Liu, L. A deep learning framework for driving behavior identification on in-vehicle CAN-BUS sensor data. *Sensors* **2019**, *19*, 1356. [CrossRef]
63. Zhang, J.; Wu, Z.; Li, F.; Luo, J.; Ren, T.; Hu, S.; Li, W.; Li, W. Attention-Based Convolutional and Recurrent Neural Networks for Driving Behavior Recognition Using Smartphone Sensor Data. *IEEE Access* **2019**, *7*, 148031–148046. [CrossRef]
64. Dos Reis, G.; Strange, C.; Yadav, M.; Li, S. Lithium-ion battery data and where to find it. *Energy AI* **2021**, *5*, 100081. [CrossRef]
65. Aguiari, D.; Chou, K.S.; Tse, R.; Pau, G. Monitoring electric vehicles on the go. In Proceedings of the 2022 IEEE 19th Annual Consumer Communications & Networking Conference (CCNC), Las Vegas, NV, USA, 8–11 January 2022; pp. 885–888.
66. Han, X.; Lu, L.; Zheng, Y.; Feng, X.; Li, Z.; Li, J.; Ouyang, M. A review on the key issues of the lithium ion battery degradation among the whole life cycle. *eTransportation* **2019**, *1*, 100005. [CrossRef]
67. Mayyas, A.; Steward, D.; Mann, M. The case for recycling: Overview and challenges in the material supply chain for automotive li-ion batteries. *Sustain. Mater. Technol.* **2019**, *19*, e00087. [CrossRef]
68. Xu, L.; Zhou, F.; Liu, B.; Zhou, H.; Zhang, Q.; Kong, J.; Wang, Q. Progress in preparation and modification of $LiNi_{0.6}Mn_{0.2}Co_{0.2}O_2$ cathode material for high energy density Li-ion batteries. *Int. J. Electrochem.* **2018**, *2018*, 6930386. [CrossRef]
69. Qi, X.; Liu, B.; Pang, J.; Yun, F.; Wang, R.; Cui, Y.; Wang, C.; Doyle-Davis, K.; Xing, C.; Fang, S.; et al. Unveiling micro internal short circuit mechanism in a 60 Ah high-energy-density Li-ion pouch cell. *Nano Energy* **2021**, *84*, 105908. [CrossRef]
70. Qi, X.; Liu, B.; Yun, F.; Wang, C.; Wang, R.; Pang, J.; Tang, H.; Quan, W.; Zhang, Q.; Yang, M.; et al. Probing heat generation and release in a 57.5 A h high-energy-density Li-ion pouch cell with a nickel-rich cathode and SiOx/graphite anode. *J. Mater. Chem. A* **2022**, *10*, 1227–1235. [CrossRef]
71. Zhang, R.; Xia, B.; Li, B.; Cao, L.; Lai, Y.; Zheng, W.; Wang, H.; Wang, W. State of the art of lithium-ion battery SOC estimation for electrical vehicles. *Energies* **2018**, *11*, 1820. [CrossRef]
72. Zhao, Y.; Patel, Y.; Hunt, I.A.; Kareh, K.M.; Holland, A.A.; Korte, C.; Dear, J.P.; Yue, Y.; Offer, G.J. Preventing lithium ion battery failure during high temperatures by externally applied compression. *J. Energy Storage* **2017**, *13*, 296–303. [CrossRef]
73. An, S.J.; Li, J.; Daniel, C.; Mohanty, D.; Nagpure, S.; Wood, D.L., III. The state of understanding of the lithium-ion-battery graphite solid electrolyte interphase (SEI) and its relationship to formation cycling. *Carbon* **2016**, *105*, 52–76. [CrossRef]
74. Balakrishnan, P.; Ramesh, R.; Kumar, T.P. Safety mechanisms in lithium-ion batteries. *J. Power Sources* **2006**, *155*, 401–414. [CrossRef]
75. Dollé, M.; Sannier, L.; Beaudoin, B.; Trentin, M.; Tarascon, J.M. Live scanning electron microscope observations of dendritic growth in lithium/polymer cells. *Electrochem. Solid-State Lett.* **2002**, *5*, A286. [CrossRef]
76. Lin, X.; Khosravinia, K.; Hu, X.; Li, J.; Lu, W. Lithium plating mechanism, detection, and mitigation in lithium-ion batteries. *Prog. Energy Combust. Sci.* **2021**, *87*, 100953. [CrossRef]
77. Reddy, M.V.; Mauger, A.; Julien, C.M.; Paolella, A.; Zaghib, K. Brief History of Early Lithium-Battery Development. *Materials* **2020**, *13*, 1884. [CrossRef] [PubMed]
78. Vetter, J.; Novák, P.; Wagner, M.; Veit, C.; Möller, K.C.; Besenhard, J.; Winter, M.; Wohlfahrt-Mehrens, M.; Vogler, C.; Hammouche, A. Ageing mechanisms in lithium-ion batteries. *J. Power Sources* **2005**, *147*, 269–281. [CrossRef]
79. Yan, P.; Zheng, J.; Gu, M.; Xiao, J.; Zhang, J.G.; Wang, C.M. Intragranular cracking as a critical barrier for high-voltage usage of layer-structured cathode for lithium-ion batteries. *Nat. Commun.* **2017**, *8*, 14101. [CrossRef]
80. Yang, R.; Mei, L.; Zhang, Q.; Fan, Y.; Shin, H.S.; Voiry, D.; Zeng, Z. High-yield production of mono-or few-layer transition metal dichalcogenide nanosheets by an electrochemical lithium ion intercalation-based exfoliation method. *Nat. Protoc.* **2022**, *17*, 358–377. [CrossRef]
81. Jie, Y.; Ren, X.; Cao, R.; Cai, W.; Jiao, S. Advanced liquid electrolytes for rechargeable Li metal batteries. *Adv. Funct. Mater.* **2020**, *30*, 1910777. [CrossRef]
82. Zhao, C.Z.; Zhao, Q.; Liu, X.; Zheng, J.; Stalin, S.; Zhang, Q.; Archer, L.A. Rechargeable lithium metal batteries with an in-built solid-state polymer electrolyte and a high voltage/loading Ni-rich layered cathode. *Adv. Mater.* **2020**, *32*, 1905629. [CrossRef]

83. Ramkumar, M.S.; Reddy, C.; Ramakrishnan, A.; Raja, K.; Pushpa, S.; Jose, S.; Jayakumar, M. Review on Li-Ion Battery with Battery Management System in Electrical Vehicle. *Adv. Mater. Sci. Eng.* **2022**, *2022*, 3379574. [CrossRef]
84. Liu, Y.; Jiang, K.; Sun, J.; Zhao, K.; Dai, J.; Wang, K. Overview of electric vehicle battery management system algorithms. In Proceedings of the 2nd International Conference on Mechanical, Electronics, and Electrical and Automation Control (METMS 2022), Guilin, China, 25 April 2022; p. 109. [CrossRef]
85. Yang, H.; Zhuang, G.V.; Ross, P.N. Thermal stability of $LiPF_6$ salt and Li-ion battery electrolytes containing $LiPF_6$. *J. Power Sources* **2006**, *161*, 573–579. . [CrossRef]
86. Lu, L.; Han, X.; Li, J.; Hua, J.; Ouyang, M. A review on the key issues for lithium-ion battery management in electric vehicles. *J. Power Sources* **2013**, *226*, 272–288. [CrossRef]
87. Campion, C.L.; Li, W.; Lucht, B.L. Thermal decomposition of LiPF6-based electrolytes for lithium-ion batteries. *J. Electrochem. Soc.* **2005**, *152*, A2327. [CrossRef]
88. Rowden, B.; Garcia-Araez, N. A review of gas evolution in lithium ion batteries. *Energy Rep.* **2020**, *6*, 10–18. [CrossRef]
89. Chou, K.S.; Aguiari, D.; Tse, R.; Tang, S.K.; Pau, G. Impact Evaluation of Driving Style on Electric Vehicle Battery based on Field Testing Result. In Proceedings of the 2023 IEEE 20th Consumer Communications & Networking Conference (CCNC), Las Vegas, NV, USA, 8–11 January 2023; pp. 1143–1146.
90. Zhao, J.; Burke, A.F. Electric Vehicle Batteries: Status and Perspectives of Data-Driven Diagnosis and Prognosis. *Batteries* **2022**, *8*, 142. [CrossRef]
91. Waldmann, T.; Wilka, M.; Kasper, M.; Fleischhammer, M.; Wohlfahrt-Mehrens, M. Temperature dependent ageing mechanisms in Lithium-ion batteries–A Post-Mortem study. *J. Power Sources* **2014**, *262*, 129–135. [CrossRef]
92. Safdari, M.; Ahmadi, R.; Sadeghzadeh, S. Numerical and experimental investigation on electric vehicles battery thermal management under New European Driving Cycle. *Appl. Energy* **2022**, *315*, 119026. [CrossRef]
93. Ben-Marzouk, M.; Pelissier, S.; Clerc, G.; Sari, A.; Venet, P. Generation of a Real-Life Battery Usage Pattern for Electrical Vehicle Application and Aging Comparison with the WLTC Profile. *IEEE Trans. Veh. Technol.* **2021**, *70*, 5618–5627. [CrossRef]
94. Kwak, B.I.; Woo, J.; Kim, H.K. Know your master: Driver Profiling-based Anti-theft method. In Proceedings of the 2016 14th Annual Conference on Privacy, Security and Trust (PST), Auckland, New Zealand, 12–14 December 2016.
95. Oh, G.; Leblanc, D.J.; Peng, H. Vehicle energy dataset (ved), a large-scale dataset for vehicle energy consumption research. *IEEE Trans. Intell. Transp. Syst.* **2020**, *23*, 3302–3312. [CrossRef]
96. Steinstraeter, M.; Buberger, J.; Trifonov, D. Battery and heating data in real driving cycles. *IEEE Dataport* **2020**. [CrossRef]
97. Petneházi, G. Recurrent neural networks for time series forecasting. *arXiv* **2019**, arXiv:1901.00069.
98. Faouzi, J. Data Set of Recurrence Plots—Pyts 0.12.0 Documentation. 2017. Available online: https://pyts.readthedocs.io/en/stable/auto_examples/image/plot_dataset_rp.html (accessed on 25 March 2023).
99. Zhou, B.; Khosla, A.; Lapedriza, A.; Oliva, A.; Torralba, A. Learning Deep Features for Discriminative Localization. In Proceedings of the 2016 IEEE Conference on Computer Vision and Pattern Recognition (CVPR), Las Vegas, NV, USA, 27–30 June 2016.

Disclaimer/Publisher's Note: The statements, opinions and data contained in all publications are solely those of the individual author(s) and contributor(s) and not of MDPI and/or the editor(s). MDPI and/or the editor(s) disclaim responsibility for any injury to people or property resulting from any ideas, methods, instructions or products referred to in the content.